JOURNAL OF SPACECRAFT AND ROCKETS
Vol. 56, No. 1, January–February 2019

Closed-Loop Control of Earth Observation Satellites

Mauricio M. Guelman* and Alexander Shiryaev†
Technion, Israel Institute of Technology, Technion City, 32000 Haifa, Israel

DOI: 10.2514/1.A34134

Low-altitude satellite orbits, while enabling high-resolution imagery of the Earth surface, have limited coverage properties. This disadvantage of the remote sensing satellites can be offset by the low-thrust electric propulsion capability, which permits to combine high-resolution with short revisit times. The purpose of this work is to present a simple closed-loop control function that allows the direct control of the orbit, making the spacecraft to pass over prescribed sites on the terrestrial surface without the need of precomputed reference trajectories. The simplicity of application contributes to the autonomy of the remote sensing satellites. The performance of the new control algorithm is illustrated by representative numerical simulation results.

Nomenclature

AU = astronomical unit, km
a = semimajor axis, km
$\boldsymbol{a}_c$ = (a_{cx}, a_{cy}, a_{cz}) commanded thrust acceleration vector
a_c = $|\boldsymbol{a}_c|$ absolute value of the commanded thrust acceleration vector, m/s^2
a_N = nominal semimajor axis, km
a_s = maximum thrust acceleration, km/s^2
a_T = commanded semimajor axis, km
C_D = spacecraft drag coefficient
C_R = spacecraft reflectivity coefficient
c_1 = control gain, s^{-1}
D = mean sidereal day
e = eccentricity
h_d = angular momentum of desired circular orbit
i = inclination, deg
K = phasing gain, s^{-1}
M = mean anomaly, deg
m = spacecraft mass, kg
n = mean motion, rad/s
n_N = nominal mean motion, rad/s
$\boldsymbol{R}$ = spacecraft heliocentric radius-vector
R = $|\boldsymbol{R}|$ magnitude of the heliocentric radius-vector, km
$\boldsymbol{r}$ = spacecraft geocentric radius vector
r = $|\boldsymbol{r}|$ magnitude of the geocentric radius vector, km
r_d = radius of the desired circular orbit, km
T_s = maximum thrust magnitude, N
t = time, s
t_T = required flyby time, s
t_i = initial time, s
u = argument of latitude, deg
u_d = desired argument of latitude at current time, deg
u_T = required argument of latitude at flyby time, deg
$\boldsymbol{u}_{\mathrm{nd}}$ = unit vector normal to the desired orbital plane
$\boldsymbol{u}_r$ = unit radius vector
$\boldsymbol{u}_T$ = unit transverse vector
$\boldsymbol{v}$ = satellite velocity vector
α = right ascension, rad
δ = declination, rad
κ = solar constant, 4.560×10^{-6}, N/m^2
λ = latitude, deg
μ = geocentric gravitational constant, 3.98601×10^5, km^3/s^2
ν = true anomaly, rad
φ = longitude, deg
ρ = atmospheric density, kg/m^3
Ω = right ascension of the ascending node (RAAN), deg
ω = argument of perigee, deg
ω_E = Earth's mean angular velocity, rad/s

Received 6 November 2017; revision received 6 May 2018; accepted for publication 20 May 2018; published online 30 July 2018.

*Emeritus Professor, Faculty of Aerospace Engineering, Asher Space Research Institute; aerglmn@technion.ac.il.
†Senior Researcher, Asher Space Research Institute.

I. Introduction

LOW-EARTH remote sensing satellites allow for smaller optical payloads, better resolution, smaller spacecraft, and less-expensive overall systems. Low altitudes also bring about undesirable perturbing forces such as higher atmospheric drag. To compensate for drag in an efficient way, an electric propulsion system with high specific impulse can be installed onboard, as was proposed in [1,2]. This makes it possible to carry out routine operations at much lower altitudes. However, because of proportionality of the swath width on the Earth's surface to the orbit height [3], the low-altitude orbits may result in a limited coverage capability. Still, the efficient use of electric propulsion (EP) can provide the means to control the orbit and to maintain its coverage capability even at low altitudes as well as reduce the amount of time needed to fly over prescribed sites.

A number of researchers have explored the possible use of EP for maneuvering the remote sensing satellites. Guelman and Kogan [4] considered minimum-propellant flight profiles for low-altitude, circular orbits, to overfly a number of selected terrestrial targets in a given time period. The maneuvering strategy, which consists of the control over the orbital period, is intended to provide the spacecraft with the ability to pass over the preselected sites at specified times. Given the site, a visiting time may be chosen only from a discrete set of opportunities that appear at the instants, when the site on the rotating Earth crosses the orbital plane. The main conclusion of their work is that EP can be effectively used to drastically reduce the revisit time of desired terrestrial targets for low-altitude missions, as compared with nonmaneuvering spacecraft. Jean and de Lafontaine [5] further the research by adding atmospheric drag and geopotential effects up to J_2 to the previous models. They start with a Sun-synchronous reference orbit and aim to return back to it after maneuvering. In essence, it is a phasing maneuver of a satellite initially at the Sun-synchronous altitude, which changes its in-orbit position by applying a thrust to gain or to lose altitude and then, by thrusting in the opposite direction, to get back to the initial altitude. The position difference between the phasing satellite and nonmaneuvering reference satellite results in the shift of the ground track. Co et al. [6,7] explore optimal thrust profiles of such in-plane maneuvers and characterize the possible changes in the ground track that can be achieved, given the EP thrust level as a function of available time. Zhang et al. [8,9] developed approximate analytical solutions for single- and dual-coplanar impulsive maneuvers, to move from initial circular/elliptical orbit to final circular/elliptical orbit, whose ground track passes over the given Earth site. The problem is solved by computing the semimajor axis of the final orbit through equating the transfer times as derived from the Kepler's

equation, and from the Greenwich mean sidereal time increment during the transfer.

The first-order optimal solutions, presented in [4,5], serve as a reference trajectory to be implemented by using some form of the orbit control. The orbit control problem, as formulated in [5], is applied to a leader-follower formation through the approach considered in [10], in which the virtual leader spacecraft is not affected by nongravitational perturbations. The reference trajectory of the virtual spacecraft is numerically propagated from the nominal orbital elements. An efficient thrusting strategy is then developed, using a control algorithm with the mean orbital elements as its inputs. Similarly, De Florio and D'Amico [11,12] consider the problem of the absolute orbit control as a specific case of two spacecraft in a formation, which includes the reference—the virtual satellite, affected only by the Earth's gravity. The control actions are implemented by means of in-plane and out-of-plane velocity increments. They introduce a new parametrization to describe the relative motion of the subsatellite points of the actual and reference satellites on the Earth's surface. Owing to this new formalization, the deviation between the actual and the reference nominal orbits can be defined in the Earth-centered, fixed coordinate frame (ECF). This approach allows the straightforward use of the modern control-theory techniques for orbit control.

A closed-loop control law was developed by Guelman [13–15] as a function of the spacecraft position and velocity with respect to the central body. It was initially designed for a transfer about small celestial bodies by continuous solar EP, and then applied to geosynchronous satellites' station-keeping. Later on, this control law was extended by Guelman and Shiryaev [16] to low-thrust spiral trajectories for low Earth orbit–geostationary Earth orbit transfer, and proved to be an effective, easy-applicable real-time solution, close to the optimal for circular-to-circular transfers under changing of both environmental conditions and the operating characteristics of real thrusters.

The purpose of this work is a further development of the algorithm for the real-time, closed-loop autonomous control of the low-altitude orbits of remote sensing spacecraft intended to fly over terrestrial targets while improving response time. The implementation of such a control will allow the direct flyover of the selected sites without the need of precomputed reference trajectories. The simplicity of application, as well as the increase of the operational flexibility and consequent reduction of the mission cost [17], should enhance the autonomy of the remote sensing satellites.

The paper is organized as follows. In Sec. II the problem is formulated, and in Sec. III the closed-loop orbit control is set forth, with the first group of simulations illustrating the development of the control algorithm. The performance evaluation is presented in Sec. IV, substantiated by the second group of simulations. Finally, in Sec. V, conclusions are given.

II. Problem Formulation

Consider a satellite in a nominal circular orbit with a period T and orbital elements $(a, e, i, \Omega, \omega, u)$—the semimajor axis, eccentricity, inclination, right ascension of the ascending node (RAAN), argument of perigee, and argument of latitude, respectively. The conditions for flyover a particular terrestrial site with geographic coordinates λ_T, φ_T—longitude and latitude—are met, when the satellite right ascension and declination (α, δ) match those of the target site (α_T, δ_T). The latter are obtained after transformation of the user-specified geographic coordinates of the target site into geocentric equatorial coordinates. Throughout the paper, the geocentric spherical and rectangular equatorial coordinates of both the satellite and target are assumed to be referred to the Earth centered inertial (ECI) J2000.0 coordinate frame, whereas the target geographic coordinates are referred to the conventional Earth centered fixed (ECF) frame. The coordinate transformation between both frames is specified by the formulas of IERS Conventions 1996 [18].

The flyby conditions are thus obtained as [19]:

$$\sin\delta_T = \sin i \sin u_T \tag{1}$$

$$\tan(\alpha_T - \Omega) = \cos i \tan u_T \tag{2}$$

where u_T is the satellite required argument of latitude at flyby time. Differences in right ascensions can be related to differences in longitudes:

$$(\alpha - \alpha_T) = (\lambda - \lambda_T) \tag{3}$$

and

$$(\alpha - \alpha_i) = (\lambda - \lambda_i) + \omega_E(t - t_i) \tag{4}$$

where index i is referred to the *initial* values of the parameters, and ω_E is the Earth's mean angular velocity.

Given a site on the terrestrial surface with geographic coordinates (φ_T, λ_T) to be covered, the time of its flyover and the corresponding argument of latitude (t_T, u_T) are defined by [5]:

$$t_T - t = \left[\arctan\frac{\sin\varphi_T \cos i}{\sqrt{\sin^2 i - \sin^2\varphi_T}} - (\lambda_T - \lambda) - \arctan(\cos i \tan u)\right] / (\omega_E - \dot{\Omega}) \tag{5}$$

$$u_T = \arcsin\frac{\sin\varphi_T}{\sin i} \tag{6}$$

where $\dot{\Omega}$ is the precession of the orbital nodes due to the Earth's oblateness. The (t_T, u_T) values are not unique, because $t_T + lD$, where D is the mean sidereal day, may be chosen instead of t_T, as well as $u_T + 2\ m\pi$ instead of u_T, with arbitrary positive integers l, m. It is here assumed that the target flyovers only occur on the descending or ascending segments of the revolution, because one of the two will typically be on the night side of the Earth.

Let's now consider a specific site, to be covered at time t_T with argument of latitude $u(t_T) = u_T$. To have the argument of latitude equal to u_T at time t_T, the desired argument of latitude u_d at current time t should be such that

$$u_d + (t_T - t)n_N = u_T + 2\pi m \tag{7}$$

where n_N is the nominal mean motion, and integer m is the number of orbital revolutions to be completed before reaching the argument of latitude u_T. Rearranging (7), we get:

$$u_d = \underset{(2\pi)}{\text{mod}}[u_T - (t_T - t)n_N] \tag{8}$$

mod being the modulo function over 2π. We shall now present a closed-loop orbit control method able to converge u to u_d within the $[t, t_T)$ time interval, so that the satellite would pass over the prescribed site on Earth at t_T, while maintaining its nominal orbital parameters.

III. Closed-Loop Orbit Control

A closed-loop orbit control provides the means to maintain the elements of the orbit, as well as to carry out the orbital maneuvers. Furthermore, similar to spacecraft attitude control, it could be fully autonomous, interacting with the ground only for monitoring performance.

In Ref. [13] a feedback control law for a transfer to a *circular* orbit was designed as a function of the spacecraft position and velocity with respect to a point-mass central body. Its development was based on two observed facts:

1) When using orbital angular momentum as a state variable, it is possible to control it by applying accelerations normal to the radius

vector, with the amplitude depending on two terms—proportional to the spacecraft velocity component normal to the radius vector, and inversely proportional to the distance from the central body.

2) To achieve a circular orbit, accelerations along the radius vector proportional to radial velocity should be added.

This planar control law, described in the Appendix, was extended to the general three-dimensional case in Refs. [14–16] as a function of the spacecraft position and velocity vectors $\boldsymbol{r}$ and $\boldsymbol{v}$ with respect to the central body. Its analytical form was defined as the control thrust acceleration vector:

$$\boldsymbol{a}_c = c_1\left(\frac{h_d}{r}\boldsymbol{u}_T - \boldsymbol{v}\right) \tag{9}$$

where $\boldsymbol{u}_T$ is the unit transverse vector:

$$\boldsymbol{u}_T = \boldsymbol{u}_{\mathrm{nd}} \times \boldsymbol{u}_r \tag{10}$$

$\boldsymbol{v} = (\dot{x}, \dot{y}, \dot{z})$, satellite velocity vector; c_1, control gain; $r = |\boldsymbol{r}|$, $\boldsymbol{r} = (x, y, z)$, satellite position vector, both $\boldsymbol{r}$ and $\boldsymbol{v}$ being referred to ECI frame; h_d, angular momentum of the desired circular orbit:

$$h_d = \sqrt{\mu r_d} \tag{11}$$

and μ is geocentric gravitational constant.

As follows from Eq. (10), vector $\boldsymbol{u}_T$ is normal to the radius vector and located in the desired orbital plane. Its direction is such that, as long as the actual orbital plane does not coincide with the desired one, a nonzero control acceleration component normal to the actual plane will be generated, to drive it to the desired plane. Once the coincidence of the planes is reached, the normal acceleration component becomes zero, and consequently $\boldsymbol{u}_T$ will lie in this plane, in the along-track direction.

Given the radius r_d and orientation vector $\boldsymbol{u}_{\mathrm{nd}}$ of the desired circular orbit, the implementation of the control law requires the current position and velocity with respect to the ECI frame.

As shown in the Appendix, in order to converge to the final circular orbit with critical damping, control gain c_1 should be chosen as

$$c_1 = 2\sqrt{\frac{\mu}{r_d^3}} \tag{12}$$

The components of the commanded acceleration on the ECI axes are expressed by the following formulas:

$$a_{xc} = -c_1\dot{x} - c_1\frac{h_d}{r^2}[y\cos i_d + z\sin i_d\cos\Omega_d] \tag{13}$$

$$a_{yc} = -c_1\dot{y} + c_1\frac{h_d}{r^2}[x\cos i_d - z\sin i_d\sin\Omega_d] \tag{14}$$

$$a_{zc} = -c_1\dot{z} + c_1\frac{h_d}{r^2}[y\sin i_d\sin\Omega_d + x\sin i_d\cos\Omega_d] \tag{15}$$

where the desired orbital plane is defined by its inclination i_d and the RAAN Ω_d. This closed-loop control law enables the satellite to transfer from any closed orbit to any circular orbit, as well as to maintain the given orbit. As was shown in [16], this control is almost optimal both with respect to the transfer time and fuel consumption for the circular-to-circular transfer.

It is worthwhile to remark that, in Eqs. (13–15), the RAAN of the target orbital plane—Ω_d—appears explicitly. For the Sun-synchronous orbit, the nodal precession, caused by the Earth's oblateness, has a significant effect, and there are two possible ways to maintain Sun synchronism—either by substitution of the current RAAN values into the control law formulae, so that the control would simply follow the natural evolution of the orbit, or by using a precomputed time-varying $\Omega_d(t)$.

A. Argument of Latitude Control

Because the argument of latitude is not affected by the closed-loop control defined by the Eqs. (13–15), a modification of the algorithm is required to enable phasing, as will be now shown.

In [14], a method was proposed to control in-orbit position by modifying the orbital radius. In [20], a similar method was introduced to correct mean anomaly error by changing the semimajor axis, and hence altering the mean motion. This method will be employed in the following.

Consider a spacecraft in a circular orbit, with its simplified kinematics expressed as

$$\frac{\mathrm{d}u}{\mathrm{d}t} = n \tag{16}$$

Then the satellite kinematics relative to the nominal orbit is

$$\frac{\mathrm{d}(\delta u)}{\mathrm{d}t} = \frac{\mathrm{d}u}{\mathrm{d}t} - \frac{\mathrm{d}u_N}{\mathrm{d}t} = n - n_N = \delta n \tag{17}$$

where

$$\delta n = \sqrt{\frac{\mu}{a^3}} - \sqrt{\frac{\mu}{a_N^3}} \tag{18}$$

To drive to zero the argument of latitude error $\delta u = u - u_d$, where u_d is given by Eq. (8), we apply the following control law:

$$\delta\dot{u} = -K\sin\delta u \tag{19}$$

where K is some positive gain, which assures stability for $u = 2n\pi$.

Combining Eqs. (18) and (19), we get:

$$-K\sin\delta u = \sqrt{\frac{\mu}{a^3}} - \sqrt{\frac{\mu}{a_N^3}} \tag{20}$$

Solving for a, we define a new commanded semimajor axis a_T, which steers the mean anomaly error to zero:

$$a_T = \mu^{1/3}\left[-K\sin(u - u_d) + \left(\frac{\mu}{a_N^3}\right)^{1/2}\right]^{-2/3} \tag{21}$$

Notice that as δu tends to zero, the new target semimajor axis goes to the original nominal value a_N.

The expressions (11) and (12) for the gains h_d and c_1 are to be updated by substituting into them a_T instead of r_d. Then the renewed control law, represented by the formulas (13–15) with the modified h_d and c_1, will make u converge to u_d.

B. Testing the Algorithm with Continuous Control

To confirm the proposed approach to the argument of latitude control and estimate the required phasing control gain K, a simulation campaign of the closed-loop control was performed with continuous thrust, as applied to the case with a nominal circular drag-free 400-km orbit ($r_{\mathrm{nom}} = 6778$ km) around the spherical Earth. The satellite is assumed to have an acceleration capability of 1 mm/s^2. The simulation initial conditions are given in Table 1.

Table 1 Simulation initial state vector

Initial moment	2012, Jan. 1, 00:00:00 UTC
Julian date	2455927.5
a, km	6778. km
E	0.0001
i, deg	98
Ω, deg	189.905
ω, deg	0.0001
M, deg	0.0001

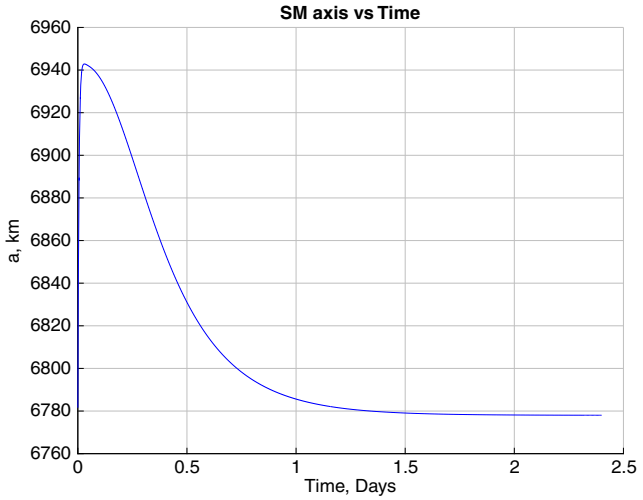

Fig. 1 Semimajor axis time history.

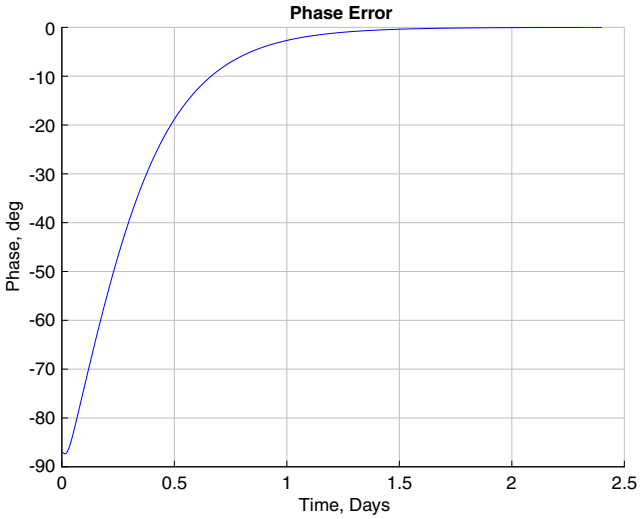

Fig. 2 Satellite argument of latitude error time history.

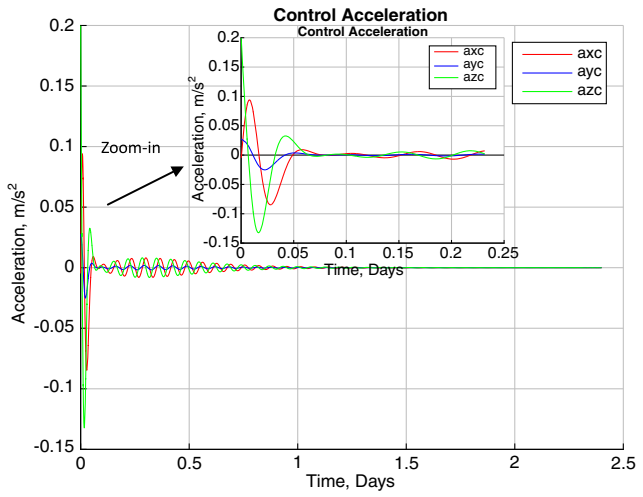

Fig. 3 Closed-loop control commanded acceleration time history.

The time and argument of latitude (t_T, u_T), as specified in formula (5), are 1.9 days and 2 rad, respectively. The results obtained in this particular case are shown in Figs. 1–3. As can be seen in Fig. 1, the semimajor axis deviates from its initial value of 6778 km to a value of 6942 km, producing a shift in the argument of latitude, displayed in Fig. 2, and bringing its initial error to zero before the required time of $t_T = 1.9$ days. The closed-loop control acceleration is plotted in Fig. 3. As a result of the numerical analysis, the gain K, defined in the formula (19), was selected equal to 4×10^{-5} s^{-1}. This choice was driven by the desire for the fastest convergence of the argument of latitude, while taking into account the limitations imposed on specific acceleration by the use of electric propulsion.

C. Constrained Thrust Magnitude

Implementation of the proposed closed-loop control is strongly dependent on the actual propulsion system configuration. Still it is important to remark that present-day electrical engines perform efficiently, when generating a fixed thrust level for a given input power. To implement the continuous, variable thrust level, as obtained from the closed-loop control for the actual EP engines, some form of discretization is required. The simplest solution is to transform thrust into an on-off function. Thrust is applied at a maximum available level T_S along the commanded direction, as prescribed by the control algorithm, whenever the commanded acceleration is above the maximum value, and put to zero otherwise:

$$\text{if } \left(a_T = \sqrt{a_{xc}^2 + a_{yc}^2 + a_{zc}^2}\right) > \left(a_S = \frac{T_S}{m}\right)$$

$$a_x = a_{xc}\left(\frac{a_S}{a_T}\right); \quad a_y = a_{yc}\left(\frac{a_S}{a_T}\right); \quad a_z = a_{zc}\left(\frac{a_S}{a_T}\right);$$

else

$$a_x = 0; \qquad a_y = 0; \qquad a_z = 0 \tag{22}$$

where m is satellite mass. The components of the commanded acceleration are referred to the ECI frame axes.

D. Adding Atmospheric Drag to the Simulation Model

For a low-altitude satellite, the acceleration caused by the atmospheric drag plays an important role. The drag acceleration is modeled as

$$\boldsymbol{a}_D = \frac{1}{2}\frac{\rho C_D S}{m} v_r \boldsymbol{v}_r \tag{23}$$

where $\boldsymbol{\rho}$ is the atmospheric density; C_D, the drag coefficient of the spacecraft; m, its mass; S, its cross-sectional area normal to the flow; and $\boldsymbol{v}_r$, its velocity relative to the atmosphere assumed to co-rotate with the Earth, with $v_r = |\boldsymbol{v}_r|$. The satellite is assumed to have a form of cannonball, so in the following simulations S parameter is set constant.

E. Testing the Algorithm with Discrete Control

The next numerical simulation was performed with the drag acceleration and control discretization included, with maximum thrust acceleration threshold a_S of 1 mm/s^2. The results are obtained with the same initial conditions, as before. The relevant satellite parameters are given in Table 2.

The time and argument of latitude (t_T, u_T), as required for fly over a given site on Earth, are $t_T = 1.9$ days and $u_T = 2$. rad. For the nominal 400-km circular orbit of the remote sensing satellite the constant atmospheric density $\boldsymbol{\rho}$ was taken equal to 6×10^{-11} kg/m^3. For $t > t_T$ phase control is discontinued. Time histories of phase error, semimajor axis, commanded acceleration, and discrete acceleration are shown in Figs. 4–7, respectively.

As can be seen in Fig. 7, at $t = 1.5$ days the commanded acceleration is below the threshold, and in fact, the satellite coasts

Table 2 Satellite parameters

Mass m, kg	100
Cross-sectional area S, m^2	1
Drag coefficient C_D	2
Reflectivity coefficient C_R	1

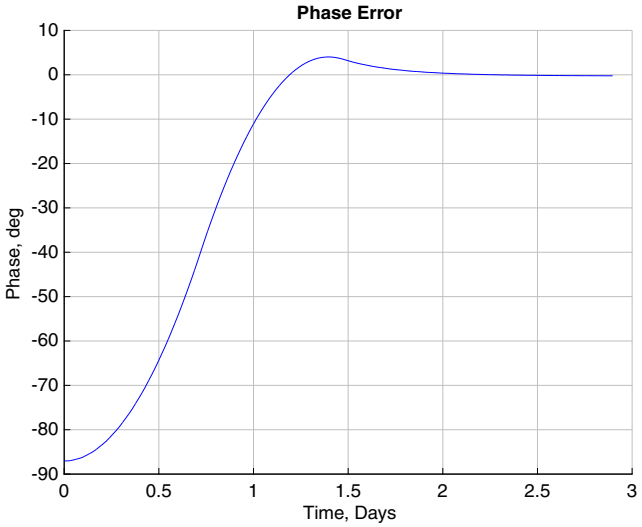

Fig. 4 Argument of latitude error time history.

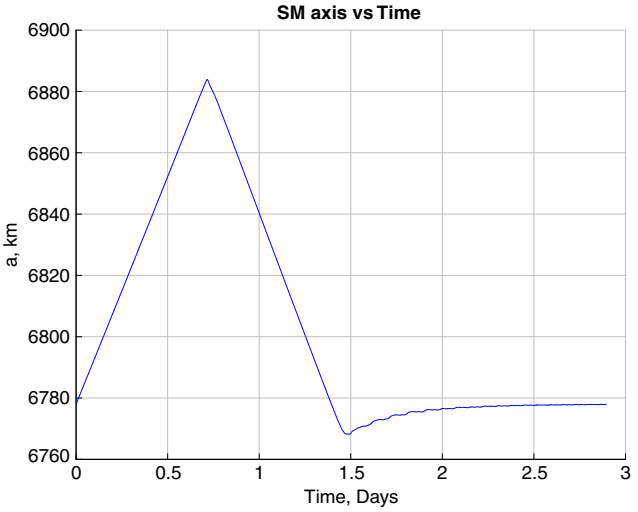

Fig. 5 Semimajor axis time history.

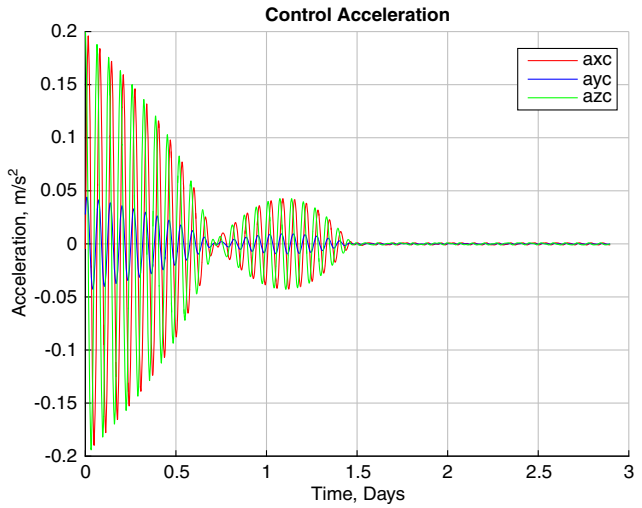

Fig. 6 Closed-loop control commanded acceleration time history.

until flyover at $t_T = 1.9$ days. The transition from phasing maneuver to nominal orbit is performed smoothly, because the same control law is applied for phasing and orbital station-keeping. Control accelerations for $t > t_T$ are still needed to compensate for the atmospheric drag.

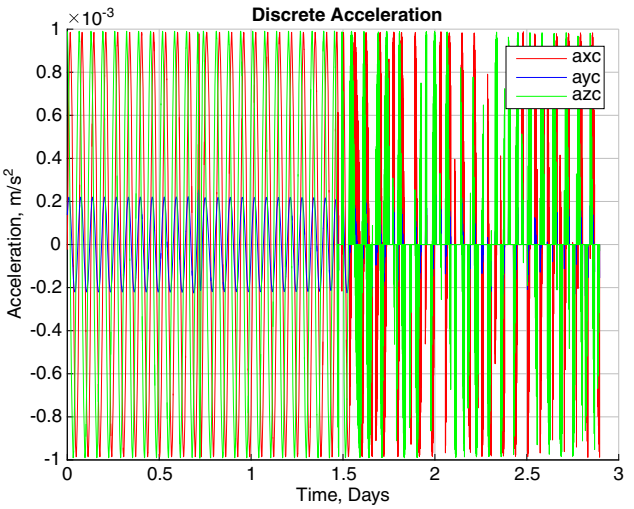

Fig. 7 Closed-loop control discrete acceleration time history.

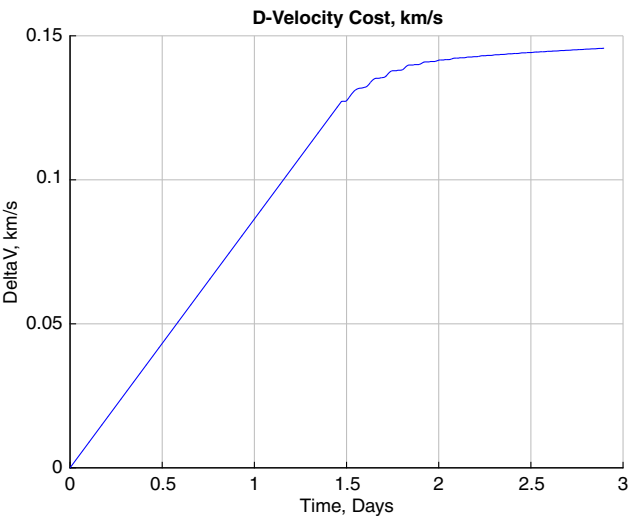

Fig. 8 ΔV Time history.

The required ΔV is shown in Fig. 8. Besides the drag compensation, it is a function of the initial error in the argument of latitude, with a minimum corresponding to a zero initial error in the argument of latitude.

F. Control in the Gravity Field of an Oblate Spheroid

As long as the orbit perturbations are much smaller than the available control acceleration, they can be easily compensated by properly augmenting the control thrust. In practice, all the perturbations, except for those caused by the J_2 term of the terrestrial gravity field, can be treated like this, at least as regard the long period and secular terms of the orbital evolution. The J_2 perturbations (as well as those caused by any other even-degree zonal harmonic) are known to drive a complex evolution of every orbital element. The evolution pattern is a superposition of secular terms, long-term oscillations with the period of rotation of apses line, and short-term oscillations with the orbital period.

To eliminate the effects of the short-term oscillations, the control law should feedback errors in terms of the mean orbital elements. Dealing with the mean elements has the advantage that short-period oscillations are not perceived as tracking errors; rather, only the long-term tracking errors are compensated for. A schematic layout of the mean element control is shown in Fig. 9. Inertial position and velocity vectors are assumed to be GPS available. Taking a Cartesian position and velocity vector, transforming it to the osculating elements, converting them to mean elements, and turning the latter elements

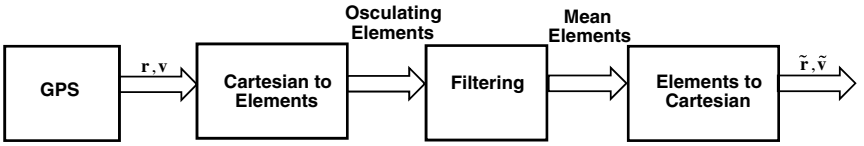

Fig. 9 Mean elements control illustration.

back into Cartesian coordinates enable to avoid tracking the short-term oscillations.

The osculating-to-mean elements' conversion was based on the Walter's iteration scheme [21,22].

IV. Performance Analysis

The evolution of a satellite under gravitational and nongravitational perturbations, when using the closed-loop control, will be now tested with a precise numerical orbit propagator [23]. The dynamical model involved in the orbit propagation includes the perturbations caused by:

1) Earth's gravity potential
2) Luni-solar gravity
3) Atmospheric drag
4) Solar radiation pressure

The models used are given in Table 3.

The acceleration due to the solar radiation pressure is calculated by the formula

$$\boldsymbol{a}_R = \kappa \left[\frac{AU}{R}\right]^2 C_R \frac{S_R}{m} \frac{\boldsymbol{R}}{R}$$

where κ is solar constant; AU, astronomical unit; $\boldsymbol{R}$, heliocentric radius-vector of the satellite; $R = |\boldsymbol{R}|$; S_R, cross-sectional area of the satellite normal to $\boldsymbol{R}$; m, satellite mass; and C_R, reflectivity coefficient. As before, the satellite is assumed to be a cannonball, so $S_R = S$.

The initial orbital elements, referred to ECI J2000.0 frame, and satellite properties are those from Tables 1 and 2. The numerical orbit propagation was carried out by RKF45 integrator.

The time and argument of latitude (t_T, u_T), as required for coverage of a given site on Earth, are $t_T = 1.9$ days and $u_T = 2$ rad, as previously. The results that include the time histories for the argument of latitude error, semimajor axis (both oscillating and mean), commanded acceleration, and discrete acceleration are shown in Figs. 10–12, respectively. The required ΔV, shown in Fig. 13, is favorably consistent with the similar result for a spherical Earth, as presented in Fig. 8.

If a set of sites is to be visited, the order of visits will strongly affect the overall fuel requirements. This explains the rationale for performing orbit design in two steps, piecewise trajectory planning and scheduling, as first presented in [4]. The first step is building piecewise trajectories that connect the pairs of sequential visiting points. Scheduling is global optimization of the trajectory by proper choice of the passage times. Because the passage times may be selected only from a discrete set of opportunities, it is a discrete optimization problem. In [4], the trajectories connecting pairs of sequential visiting sites were based on explicit formulas of piecewise optimization. When using the closed-loop control, as here presented, the same process can be applied with the minimization only considering the order of visiting sites.

Table 3 The standard models used in the force function

Model	Name
Geopotential model	EGM96 (70×70)
Ephemerides of the Sun, Moon, and major planets	DE405/LE405
Atmospheric density model	NRLMSISE-00
Solid Earth tides	Wahr's theory [18]
Ocean tides	CSR3.0

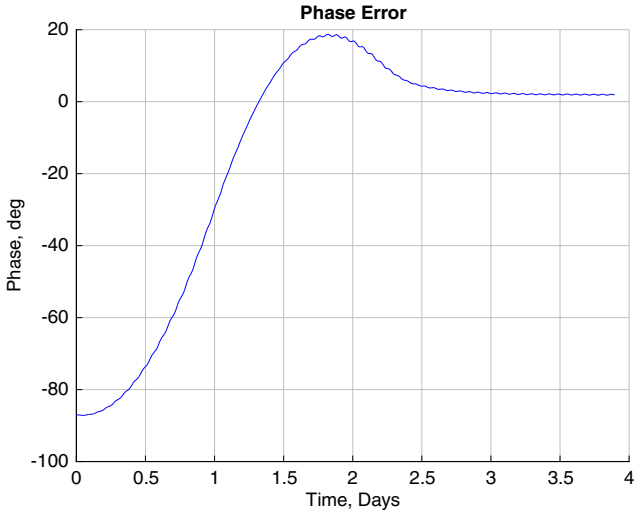

Fig. 10 Argument of latitude' error time history, with mean elements in the control law.

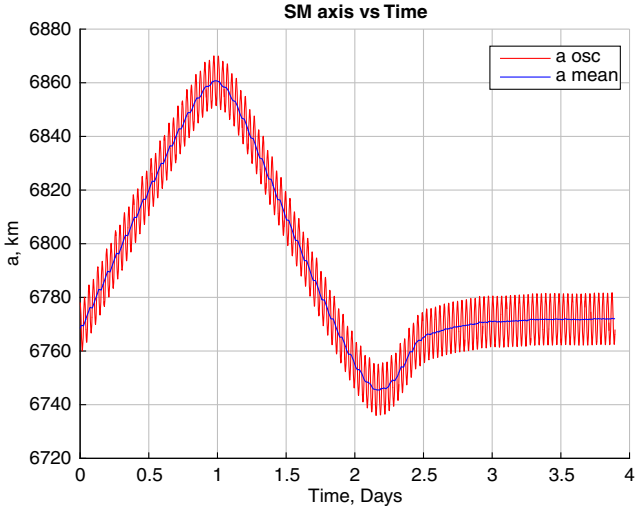

Fig. 11 Semimajor axis time history.

It should be noted that connection between successive partial trajectories is smoothly performed, because at the end of each arc connecting two sites, the satellite returns to its *nominal circular orbit*. This will be now demonstrated with an example similar to the case presented in [24], with visits to a set of 10 sites presented in Table 4.

Based on present developments of electric propulsion systems, a single thruster of the type developed by the Keldish Research Center (Russia) [25] or a cluster of three CAM200 small thrusters developed by Rafael (Israel) [26] with characteristics presented in Table 5 may be used. In both cases a total thrust of 40 mN is assumed and for a 100 kg satellite mass the acceleration capability of 0.4 mm/s^2 is now implemented.

Given an initial date of 1 January 2012 at 00:00:00 UTC with initial state vector specified in Table 1, the satellite is tasked to overfly the selected targets. Once the ground track intersects the first target,

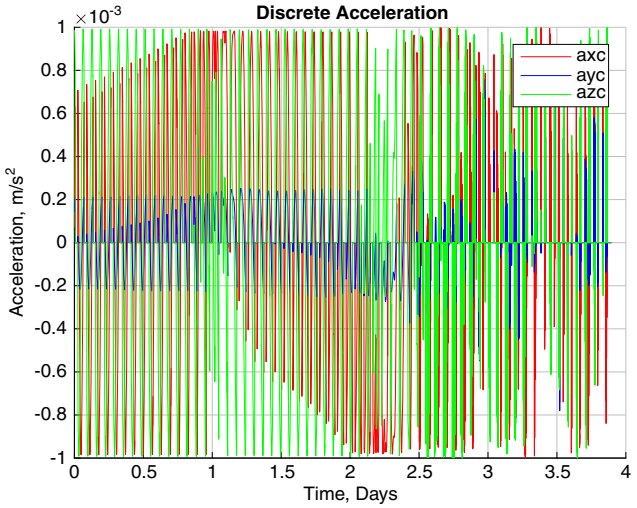

Fig. 12 Closed-loop control discrete acceleration time history, with mean elements in the control law.

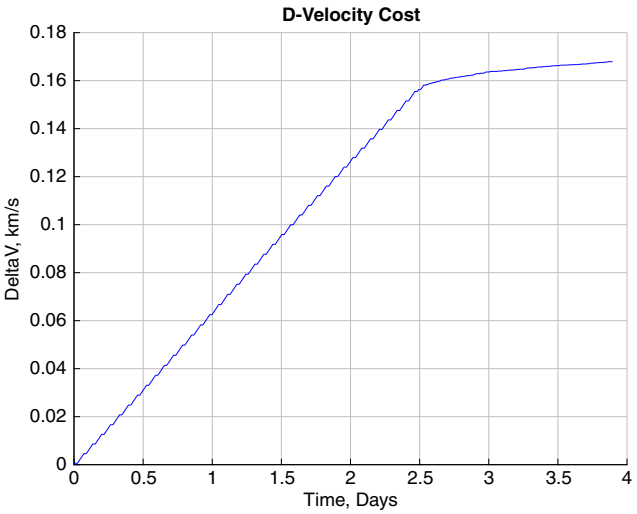

Fig. 13 ΔV time history with mean elements in the control law.

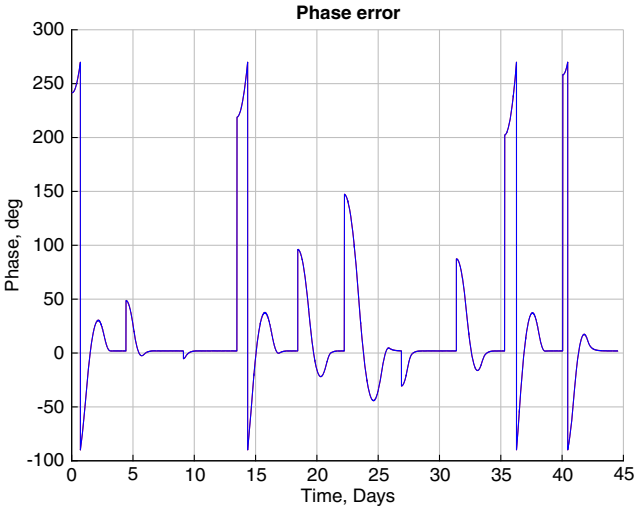

Fig. 14 Argument of latitude' error time history (10 sites flyover, with eclipse EP interruption).

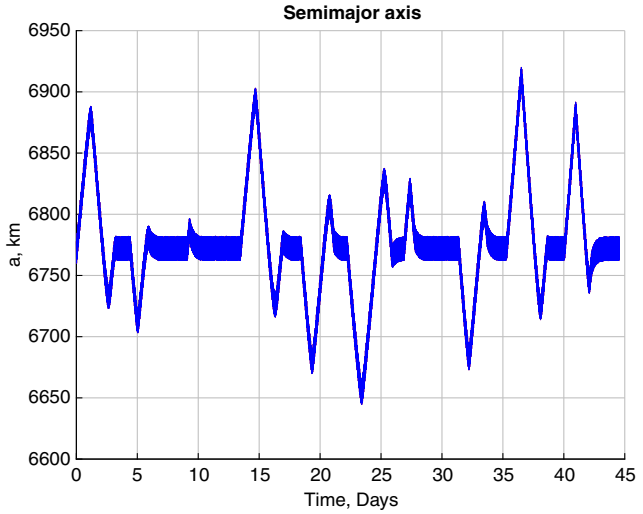

Fig. 15 Semimajor axis time history (10 sites flyover, with eclipse EP interruption).

the vehicle is tasked to overfly the next one without prior knowledge of the target list. This process is repeated until all 10 targets are visited. As previously indicated, the order and location of the targets relative to the other sites will have an impact on the total required ΔV; however, this is beyond the scope of the present paper.

Table 4 Ten randomly selected targets by location and order

Location	Latitude	Longitude
1. Washington, D.C.	38°53′ N	282°58′ E
2. Berlin, Germany	52°30′ N	13°25′ E
3. Tokyo, Japan	35°40′ N	139°45′ E
4. Ottawa, Canada	45°24′ N	284°17′ E
5. Madrid, Spain	40°26′ N	356°18′ E
6. Moscow, Russia	55°45′ N	37°36′ E
7. Beijing, China	39°55′ N	116°25′ E
8. Canberra, Australia	35°17′ S	149°08′ E
9. Cairo, Egypt	30°02′ N	31°21′ E
10. Brasilia, Brazil	15°48′ S	312°06′ E

Table 5 Parameters of some existing EP thrusters

Type	KM-60	CAM200
Power, W	450–900	100–250
Thrust, mN	23–44	6–14
Specific impulse, s	1700–2200	900–1500

The process of the sites' flyover is performed as follows. The latitude and longitude of the first site are used to compute the corresponding possible times $t_T + lD$ and argument of latitude u_T, as given by Eqs. (5) and (6). Because convergence time is not fixed in advance, the error in the argument of latitude at possible times $t_T + lD, (l = 1, 2, \ldots)$ of the site crossing the satellite orbital plane, is checked, and if found less than the prescribed value, the site is assumed to be covered. The satellite is then tasked to overfly the next site, repeating the same process.

The time history graphs in the Figs. 14–16 pertain to the flyover of the 10 targets given in Table 4.

This simulation uses now a proper atmospheric drag model. Furthermore, during the eclipses the EP thrusting ceases, so the convergence time increases.

As can be seen in Fig. 15, where the semimajor axis time history is presented the closed-loop control achieves the flyover of the target sites by either reducing or increasing the orbit altitude. It is worth mentioning that all sites are overflown at the *same nominal altitude*, providing thus the same resolution. Figure 16 shows the required ΔV.

Remarks:

1) The example here presented assumes that only one of the orbit ascending or descending arcs is available for sensing due to illumination requirements. For remote sensing systems, independent

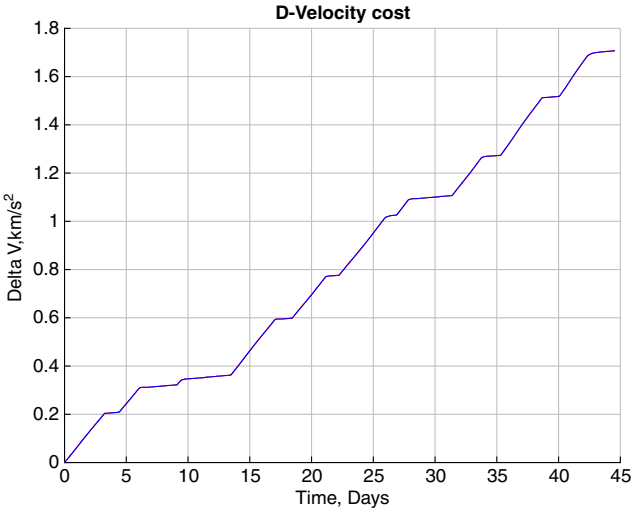

Fig. 16 ΔV time history (10 sites flyover, eclipse EP interruption).

of illumination requirements, both arcs can be used, with possible significant reduction in transition time from site to site.

2) The closed-loop control allows for fully autonomous operation of the satellite. There is no need for planning or precomputed orbits, the only information to be transmitted to the onboard system are the sites coordinates, and the entire process can be straightforwardly implemented.

V. Conclusions

Closed-loop control of remote sensing satellites was presented. The feasibility of the proposed approach has been validated in a detailed simulation study. It was shown that the spacecraft flight over prescribed Earth sites could be performed in a precise manner without the need of a precomputed reference orbit.

The closed-loop control is of simple and direct implementation, requiring the real-time knowledge of the spacecraft position and velocity with respect to the Earth. The closed-loop control is an effective real-time solution with all well-known characteristics of feedback solutions. It is robust, needs no lengthy and complex optimization, naturally copes with unmodeled effects, and is changing operating characteristics of real propulsion systems.

This closed-loop control law here presented enables the satellite to overfly prescribed sites while maintaining the nominal orbit characteristics, because the same control applies both for phasing and station-keeping. The case of visiting a set of sites was here considered without regard to the order and location of the targets relative to the other sites. Because this order has a significant impact on the overall fuel requirements, it will be the subject of future research, integrating the closed loop control here presented with an optimization scheduling routine.

Appendix: Planar Closed Loop Control for Orbit Transfer

We will consider the equatorial plane orbit transfer about a point-mass central body with gravitational constant μ. The spacecraft is assumed to be able to control thrust continuously.

The equations of motion in polar coordinates are given by

$$r\ddot{\theta} + 2\dot{r}\,\dot{\theta} = a_\theta \tag{A1}$$

$$\ddot{r} - r\dot{\theta}^2 = a_r - \frac{\mu}{r^2} \tag{A2}$$

where a_θ and a_r are the tangential and radial components of the thrust acceleration.

Let us now define the following control law for orbit transfer:

$$a_\theta = -c_1\left(r\dot{\theta} - \frac{h_e}{r}\right) \tag{A3}$$

$$a_r = -c_1\dot{r} \tag{A4}$$

where c_1 and h_e are control constants.

Introducing (A3) and (A4) into the equations of motion (A1) and (A2) and employing as state variables $h = r^2\dot{\theta}$, r, $\dot{r}$, the following nonlinear third order system is obtained:

$$\dot{h} = -c_1(h - h_e) \tag{A5}$$

$$\ddot{r} = -c_1\dot{r} + \frac{h^2}{r^3} - \frac{\mu}{r^2} \tag{A6}$$

The system equilibrium points are given by

$$h = h_e \tag{A7}$$

$$\mu r_e - h_e^2 = 0 \tag{A8}$$

The system has a single equilibrium point corresponding to a circular orbit with radius $r = r_e$ and angular momentum h_e.

The system behavior can be analyzed by linearizing it about the equilibrium point,

$$\delta\dot{h} + c_1\delta h = 0 \tag{A9}$$

$$\delta\ddot{r} + c_1\delta\dot{r} + \frac{\mu}{r_e^3}\delta r - \frac{2h_e}{r_e^3}\delta h = 0 \tag{A10}$$

The single equilibrium point ($h = h_e$, $r = r_e$) is stable for all positive guidance gains c_1.

A stable equilibrium point implies that for $t \to \infty$, $r = r_e$, $\dot{r}_e = 0$, $h = h_e$. That is, the final orbit is *circular* with angular momentum h_e and radius r_e.

For the case that the required final orbit is circular with radius r_d, the guidance constant h_e is defined such that

$$h_e = h_d = \sqrt{\mu r_d} \tag{A11}$$

Furthermore, the trajectory will converge to the final circular orbit with critical damping, provided

$$c_1 = 2\sqrt{\frac{\mu}{r_e^3}} \tag{A12}$$

References

[1] Fearn, D. G., "High Resolution Optimal Remote Sensing from a 200 kg-Class Spacecraft," *45th Congress of the International Astronautical Federation*, IAF Paper 94-B.2.072, Jerusalem, Oct. 1994.

[2] Guelman, M., and Psiaki, M. L., "Electric Propulsion for Orbit Transfer in a Resistive Medium," *Journal of the Astronautical Sciences*, Vol. 44, No. 1, Jan.–March 1996, pp. 79–97.

[3] Elachi, C., *Introduction to the Physics and Techniques of Remote Sensing*, Wiley, New York, 1987, pp. 393–404.

[4] Guelman, M., and Kogan, A., "Electric Propulsion for Remote Sensing from Low Orbits," *Journal of Guidance, Control, and Dynamics*, Vol. 22, No. 2, 1999, pp. 313–321. doi:10.2514/2.4380

[5] Jean, I., and de Lafontaine, J., "Autonomous Guidance and Control of an Earth Observation Satellite Using Low Thrust," *Advances in the Astronautical Sciences*, AAS Paper 03-617, 2003, pp. 1829–1844.

[6] Co, T. C., Zagaris, C., and Black, J. T., "Satellite Responsiveness Using In- and Out-of-Plane Maneuvering," *Reinventing Space Conference*, AIAA Paper RS-2012-3004, May 2012.

[7] Co, T. C., Zagaris, C., and Black, J. T., "Responsive Satellites Through Ground Track Manipulation Using Existing Technology,"

Journal of Spacecraft and Rockets, Vol. 50, No. 1, 2013, pp. 206–216.
doi:10.2514/1.A32263

[8] Zhang, G., Cao, X., and Mortari, D., "Analytical Approximate Solutions to Ground Track Adjustment for Responsive Space," *IEEE Transactions on Aerospace and Electronic Systems*, Vol. 52, No. 3, June 2016, pp. 1366–1383.
doi:10.1109/TAES.2016.140644

[9] Zhang, G., and Sheng, J., "Impulsive Ground-Track Adjustment for Assigned Final Orbit," *Journal of Spacecraft and Rockets*, Vol. 53, No. 4, 2016, pp. 599–609.
doi:10.2514/1.A33447

[10] Zeiler, O., Schubert, A., Häusler, B., and Puls, J., "Autonomous Orbit Control for Earth-Observation Satellites," *4th ESA International Conference on Spacecraft Guidance, Navigation and Control Systems*, ESA, Noordwijk, The Netherlands, Oct. 1999, pp. 189–194.

[11] De Florio, S., and D'Amico, S., "Optimal Autonomous Orbit Control of a Remote Sensing Spacecraft," *Spaceflight Mechanics 2009*, Advances in the Astronautical Sciences Series, Vol. 134, Univelt, San Diego, CA, 2009, pp. 949–968.

[12] De Florio, S., D'Amico, S., and Radice, G., "Virtual Formation Method for Precise Autonomous Absolute Orbit Control," *Journal of Guidance, Control, and Dynamics*, Vol. 37, No. 2, 2014, pp. 425–438.
doi:10.2514/1.61575

[13] Guelman, M., "Dynamics and Control of Close Orbits Around Small Rotating Bodies," *Proceedings of the AAS/AIAA Space Flight Mechanics Conference*, AAS Paper 97-103, 1997.

[14] Guelman, M., "Geostationary Satellites Autonomous Closed Loop Station Keeping," *Acta Astronautica*, Vol. 97, April–May 2014, pp. 9–15.
doi:10.1016/j.actaastro.2013.12.009

[15] Guelman, M., "Closed-Loop Control of Close Orbits Around Asteroids," *Journal of Guidance, Control, and Dynamics*, Vol. 38, No. 5, 2015, pp. 854–860.
doi:10.2514/1.G000158

[16] Guelman, M., and Shiryaev, A., "Closed-Loop Orbit Transfer Using Solar Electric Propulsion," *Journal of Guidance, Control, and Dynamics*, Vol. 39, No. 11, 2016, pp. 2563–2569.
doi:10.2514/1.G000395

[17] Gurevich, G., Bell, R., and Wertz, J. R., "Autonomous On-Board Orbit Control: Flight Results and Applications," *AIAA 2000 Conference and Exposition*, AIAA Paper 2000-5226, Sept. 2000.

[18] McCarthy, D. D., (ed.), *IERS Conventions (1996)*, 1996, Observatoire de Paris, https://www.iers.org/IERS/EN/Publications/TechnicalNotes/tn21.html.

[19] Battin, R. H., *An Introduction to the Mathematics and Methods of Astrodynamics*, AIAA Education Series, AIAA, New York, 1987, pp. 123–125.

[20] Naasz, B. J., "Classical Element Feedback Control for Spacecraft Orbital Maneuvers," Master's Thesis, Virginia Polytechnic Inst. and State Univ., Blacksburg, VA, 2002.

[21] Walter, H. G., "Conversion of Osculating Orbital Elements into Mean Elements," *The Astronomical Journal*, Vol. 72, No. 8, 1967, pp. 994–997.
doi:10.1086/110374

[22] Long, A. C., et al., "Goddard Trajectory Determination System (GTDS)," Mathematical Theory, Rev. 1, July 1989, pp. 5-54–5-63, http://www.ltas-vis.ulg.ac.be/cmsms/uploads/File/GoddardTrajectorySystem.pdf.

[23] Shiryaev, A., "Testing the Orbit Determination Algorithm by the Satellite Laser Ranging Measurements," *Proceedings of the 48th Israel Annual Conference on Aerospace Sciences*, Technion–I.I.T., Haifa, Israel, March 2008.

[24] Co, T. C., and Black, J. T., "Responsiveness in Low Orbits Using Electric Propulsion," *Journal of Spacecraft and Rockets*, Vol. 51, No. 3, May–June 2014, pp. 938–945.
doi:10.2514/1.A32405

[25] Murashko, V., et al., "State of the Art and Prospects of Electric Propulsion in Russia," *IEPC-03-340, 28th International Electric Propulsion Conference*, Toulouse, France, March 2003, http://erps.spacegrant.org/uploads/images/images/iepc_articledownload_1988-2007/2003index/0340-0303iepc-full.pdf.

[26] Franco, D. K., Lev, D., and Appel, L., "Recent Development of the CAM200 Low Power Hall Thruster," *35th International Electric Propulsion Conference, IEPC-2017-247*, Georgia Institute of Technology, Atlanta, GA, Oct. 2017, https://iepc2017.org/sites/default/files/speaker-papers/recent_development_of_the_cam200_low_power_hall_thruster_-_iepc2017_-_final.pdf.

M. Xin
Associate Editor